Atmospheric Environment 169 (2017) 297–306

Contents lists available at ScienceDirect

Atmospheric Environment

journal homepage: www.elsevier.com/locate/atmosenv

IMAA (Integrated Measurements of Aerosol in Agri valley) campaign: Multi-instrumental observations at the largest European oil/gas pre-treatment plant area

Mariarosaria Calvello [a, *], Rosa Caggiano [a], Francesco Esposito [b], Antonio Lettino [a], Serena Sabia [a], Vito Summa [a], Giulia Pavese [a]

[a] Consiglio Nazionale delle Ricerche- Istituto di Metodologie per l'Analisi Ambientale (CNR-IMAA), C. da S. Loja, 85050 Tito Scalo, Potenza, Italy
[b] Università della Basilicata - Scuola di Ingegneria, C. da Macchia Romana, 85100 Potenza, Italy

HIGHLIGHTS

- First multi-instrumental experiment at the largest European oil/gas pre-treatment plant area.
- Integrated approach for aerosol characterization at the ground and over the column.
- S, Ni and Zn found as tracers of the plant emissions.
- SO_2 and CH_4 emissions strongly influence the state of mixing of particles.
- A relevant contribution of EBC to the total number of fine particles.

GRAPHICAL ABSTRACT

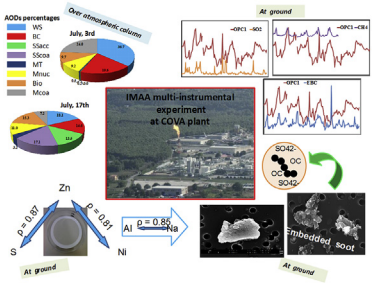

ARTICLE INFO

Article history:
Received 29 March 2017
Received in revised form
13 September 2017
Accepted 16 September 2017
Available online 20 September 2017

Keywords:
Multi-instrumental campaign
Oil extraction and pre-treatment
Aerosol characterization

ABSTRACT

A short-term intensive multi-instrumental measurement campaign (Integrated Measurements of Aerosol in Agri valley - IMAA) was carried out near the largest European oil and gas pre-treatment plant (Centro Olio Val d'Agri - COVA) in a populated area, where, so far, ample characterization of aerosol loading is missing. As such, between the 2 and 17 July in 2013, using a number of instruments analyses were carried out on physical, chemical, morphological and optical properties of aerosol at this distinctive site, at both ground and over the atmospheric column, including the investigation of the mixing and transformation of particles. The observation of slag silicates with a rough surface texture is consistent with the presence of oil-related activities which represent the only industrial activity in the area. Desulfurization/sulfur liquefaction processes occurring at COVA can explain the peculiar morphology of calcium-sodium-aluminum particles. The common COVA source was associated with high concentrations of sulfur, nickel and zinc, and with significant correlations between zinc-sulfur and zinc-nickel. The Optical Particle Sizer (OPS) data, hygroscopicity and optical properties of atmospheric aerosol are consistent with the typical oil-derived gaseous emissions (e.g. sulfur dioxide and methane) that strongly influence the mixing state of particles and their size distributions. Continuous combustion processes at COVA were found to be responsible for Equivalent Black Carbon (EBC) concentrations from their relevant contribution to the total number of fine particles. The expected significant contribution of WS (water soluble)

* Corresponding author.
E-mail address: mariarosaria.calvello@imaa.cnr.it (M. Calvello).

https://doi.org/10.1016/j.atmosenv.2017.09.026

and BC (Black Carbon) components to the total Aerosol Optical Depth (AOD) are consistent with the results from the radiometric model especially for July 3 and 16.

1. Introduction

The presence of one of the largest European on shore oil fields and the largest crude oil and gas pre-treatment plant (COVA) in a populated area prompted interest in studying aerosol optical, chemical and morphological properties in the Agri Valley, Southern Italy. The oil field and the COVA plant are in a rural area with agricultural and grazing activities, a large biodiverse woods and mountain ecosystem, and a population of about 50,000 divided between a few small towns.

Environment and health issues relating to combustion processes, extraction and pre-treatment of oil and gas at COVA, including traffic from heavy vehicles, needs to be addressed in order to further understand the potential impact on the area. In fact, anthropogenic emissions can be responsible for negative effects on air quality, public health and the climate (Andreae et al., 2005; Dockery, 2001; Jacobson and Streets, 2009; Koch and Del Genio, 2010; Morawska and Zhang, 2002). Moreover, due to the high temporal and spatial variability of aerosols in the atmosphere, a comprehensive approach investigating emitted particle concentrations, dimensions, chemical composition, optical properties, morphology, mixing and transformation processes is necessary to effectively assess their sources and effects.

So far the number of studies on aerosol emissions from oil/gas treatment activities has mainly been focused on refineries (Baltrėnas et al., 2011; Lin et al., 2004; Sarnela et al., 2015) and gas production facilities (Rutter et al., 2015; Warneke et al., 2014; Zielinska et al., 2014). Most of the results from these studies have helped to assess the role of gaseous compounds, particularly VOCs, BTEX and PAHs (Lopes Oliveira et al., 2014; Sakari, 2012) however, not enough information is available on the aerosol fraction.

Additionally, recent papers/studies on carbonaceous aerosol emissions from flaring have assessed the importance of such contribution to the Black Carbon (BC) global load, estimated to be 4% of the total BC (Fawole et al., 2016; Stohl et al., 2013). With reference to the Agri Valley, Margiotta et al. (2015). Scanning Electron Microscope (SEM) analysis on PM_1 filters during and after a burning torch flare event at the COVA plant, is consistent with the production of a large amount or soot from flaring.

Other previous studies on aerosols in the Agri Valley, on both PM_1 (Speranza et al., 2014; Trippetta et al., 2014) and on BC datasets (Calvello et al., 2015; Pavese et al., 2012), highlighted the influence of extraction and pre-treatment activities on air quality. The main findings highlighted this unique area, with PM concentrations comparable to those in urban sites, and a relevant contribution of BC to total aerosol loading despite the rural nature of the site.

The present work endeavors to combine different measurements and techniques to produce the first set of integrated data on optical, physical, chemical and morphological properties of aerosols in the Agri Valley. This study aims to obtain an extensive characterization of aerosol loading at the site and explore the mixing, aging and transformation of particles due to the key role of these processes in modifying aerosol impacts on health and the environment (Cheng et al., 2015; Künzi et al., 2013; Rager et al., 2011). In this respect, useful results were obtained at the Habshan industrial site for oil and gas production by Semeniuk et al. (2015), where changes in reflectivity, scattering, particles size, hygroscopicity and ice nucleation properties of processed aerosols were observed.

Data collected on July 2013 during the short-term intensive multi-instrumental campaign IMAA were analyzed on two different temporal scales (24 h/1 h) and on different dimensional ranges, to follow particles formation processes. In particular, in-situ gravimetric sampling, chemical speciation, and SEM-EDX (Energy Dispersive X-ray) analysis were performed on $PM_{2.5}$ collected on a 24 h basis; EBC, OPS derived size-distributions (0.3–10 μm) and concentrations of many gaseous compounds were obtained with an hourly temporal resolution. To complete the study, columnar-integrated AODs, Ångström turbidity parameters and aerosol number and volume size distributions were determined using radiometric measurements. Measured AODs were the input of a suitable technique that allowed to estimate the main aerosol columnar components contributing to the solar radiation attenuation. Possible correlations between ground-measured EBC concentrations and columnar BC contribution to the total AODs were investigated.

2. COVA plant: site and processes description

The IMAA measurements campaign was held in the Agri Valley, a rural area surrounded by the “Appennino Lucano Val d'Agri Lagonegrese” National Park. It hosts one of Europe's' biggest onshore oil fields with 27 oil wells, that were producing about 82,000 barrels of oil equivalent (BOE) per day when the study was conducted (ENI, 2014) and the largest pre-treatment oil plant (170,000 m^2) “ENI Centro Olio Val d'Agri” (COVA, 40.68°N, 15.53°E). This area, traversed by the SS598 main road, houses a few villages with about 50,000 inhabitants. The instruments were located very close to the plant (less than 400 m from the security torches and about 500 m from the incinerators). Fig. 1a shows a map of the COVA plant and the measurement site. The crude oil from both Val d'Agri and Monte Alpi productions is processed at COVA, to separating the three phases; treated crude oil, gas and water. The main processes undertaken in this area are: gas desulfurization using hydrogen sulfide dissolution into methyl-dietanolamine (MDEA), H_2S conversion into liquid S by Claus process and SCOT (Shell Claus off-gas treatment) process, and gas dehydration (Prefettura Potenza, 2013). The Claus process is coupled with the SCOT process for gas tail treatment and mainly consists of the partial combustion of the hydrogen sulfide-rich gas stream and the subsequent reaction of the unburnt hydrogen sulfide with the sulfur dioxide in the presence of alumina catalyst to produce elemental sulfur (EU-JRC-IPTS, 2015).

Gas dehydration occurs by means of triethylene glycol (TEG) or by alumina beds depending on the different characteristics of processed crude oil. The regenerating TEG process leads to the production of water, CO_2 and light hydrocarbon vapors which are burnt within the incinerators. Some more emissions can be derived from the process water that, with a high content of salts, oil, suspended solids and gas, is treated to separate oil from gas which is finally sent to the incinerator (Prefettura Potenza, 2013).

It is important to note that details on processes cycles at the COVA plant are unknown, resulting in an expected high variability in emissions.

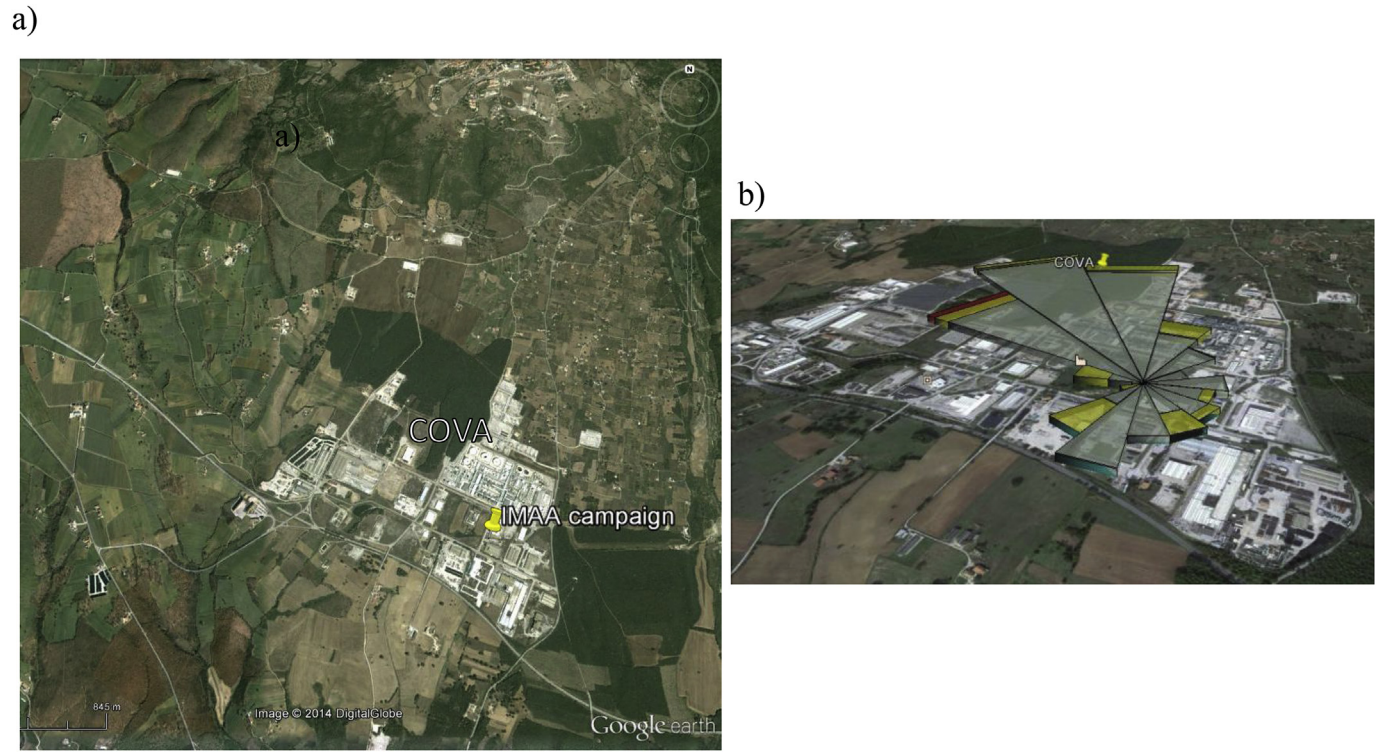

Fig. 1. Location of the COVA plant and of the measurement site (a). Wind rose calculated for the period July 2–17 overlapping the COVA plant (b). Aerial maps courtesy of Google Earth (http://earth.google.com).

3. Instruments and methods

A mobile laboratory was set up in COVA (Fig. 1a) to carry out an intensive field campaign using a multi-instrumental approach to study physical, chemical, morphological and optical properties in atmospheric aerosols from 2 to 17 July 2013.

$PM_{2.5}$ aerosol particles were collected using a low volume (16.7 l min-1 flow rate) gravimetric sampler (TCR Tecora) on polycarbonate filters (Ø = 47 mm). The sampling time was 24 h (starting from 12:00 p.m.), and each filter was humidity-conditioned in a filter-conditioning cabinet (T = 20 ± 2 °C and RH = 50 ± 5%) before and after sampling for 48 h. The $PM_{2.5}$ mass was determined using a gravimetric method and an analytical microbalance with a sensitivity of ±1 μg. To determine trace elements content in $PM_{2.5}$ samples, filters were acidic digested following the chemical protocol described in Caggiano et al. (2001). The total concentrations of seventeen trace elements were measured using an Inductively Coupled Plasma Optical Emission Spectrometry (ICP-OES, Varian - Vista MPX) or an Atomic Absorption Spectrometry Furnace Graphite (GFAAS).

The method detection limit (MDL) was used to determine the lowest concentration level that can be detected as statistically different from a blank. The efficiency of the extraction procedure was tested using the National Institute of Standard and Technology (NIST) standard reference material Urban Particulate Matter, SRM 1 648. Recovery efficiencies were in the range of the certified standard. Trace element recovery percentages were found within the ranges of 100 ± 15%, and the blank contribution was found to be <10% of the measured values.

$PM_{2.5}$ samples were also analyzed using a field emission scanning electron microscope (FESEM) equipped with an Energy Dispersive X-ray Spectrometer (EDS, Oxford Inca Energy 350). A small portion (0.5 cm^2) of the filter was attached to an aluminum stub using a carbon sticky tab and was subsequently carbon coated. The samples were examined using images taken by secondary electron (SE) and back-scattered electron (BSE) detectors. For each sample a total of 350 particles with a diameter of more than 400 nm was manually analyzed and classified based on both their morphology and chemical compositions. Although the EDS was equipped with an ultrathin window to allow direct analysis of carbon and oxygen, only elements with Z > 10 (Na) were considered in the X-ray spectra evaluation as the samples were graphite-coated, and carbon and oxygen were present in the polycarbonate filters.

An optical particle sizer, TSI 3 330 OPS, working at a flow rate of 1 Lm^{-1}, was used to detect particles in 16 channels, from 0.3 to 10 μm in diameter, to obtain the size distribution of particle number concentrations with a time resolution of 5 min.

EBC content was determined using a Rack-Mount 7-wavelengths Magee Scientific aethalometer AE31 (λ = 370, 470, 520, 590, 660, 880, 950 nm), which measures the attenuation of light transmitted from seven lamps due to the absorption properties of carbonaceous aerosol collected on the quartz fiber filter. EBC concentrations were derived from the absorption coefficients σ_{aer} measured at the 7 wavelengths, assuming a mass absorption cross section (MAC) inversely proportional to the wavelength (Hansen, 2005). A value of 16.6 m^2g^{-1} was used for MAC at 880 nm. The instrument was set with a cut size-selective cyclone for particles with aerodynamic diameters of less than 2.5 μm, a flow rate of 4 L/min, and a time-resolution of 5 min. To minimize the shadowing effect, a tape advancing time of 1 h was chosen (Calvello et al., 2015). No correction for the scattering effect was performed due to lack of contemporary scattering measurements, thus leading to a possible overestimation in the absolute EBC values.

Continuous and near-real-time measurements of the concentrations of several gaseous compounds were provided by the

Agenzia Regionale per la Protezione dell'Ambiente (ARPA) Basilicata monitoring station, Viggiano Zona Industriale (VZI, 40.18°N, 15.54°E, 565 m a.s.l). In particular concentrations of sulfur dioxide (SO_2), carbon monoxide (CO), nitrogen dioxide (NO_2), hydrogen sulfide (H_2S), methane (CH_4), non-methane hydrocarbons (NMHCs), benzene (C_6H_6), and toluene were considered for this study. In addition, the main meteorological parameters i.e air temperature (T), relative humidity (RH), atmospheric pressure (P) and global radiation (GR), wind direction (wd, Fig. 1b), wind speed (ws) and rainfall (rf) were provided. A detailed description of the measurement methods used at the VZI station is reported in Calvello et al. (2014).

Ground based columnar measurements were carried out using a high resolution (1.5 nm) S2000 Ocean Optics spectro - radiometer (spectral range 400 nm–800 nm), in cloudless conditions, with a time resolution of 15 min. The parameters estimated by measuring the attenuation of solar direct irradiance at ground level were AOD, Ångström exponent (alpha) and aerosol number and volume size distributions. In particular, the estimated AODs were used as inputs in a suitable technique, based on the aerosol components from the OPAC (Optical Properties of Aerosols and Clouds) model, to estimate the contribution of different atmospheric aerosol components using a minimization procedure (Pavese et al., 2016). According to this technique, total optical depth is expressed as a linear combination of the partial optical depths corresponding to each of the eight OPAC components, i.e water soluble (WS), Black Carbon (BC), sea salt coarse mode (SScoa), sea salt accumulation mode (SSacc), mineral transported (MT), mineral nucleation (Mnuc), biogenic (Bio) and mineral coarse (Mcoa).

To support data interpretation, trajectories analysis were performed using a HYSPLIT4 (Draxler and Rolph, 2003). Back-trajectories were calculated for each day in order to obtain an overview of the main aerosol transport phenomena.

Aerosol property analysis was performed on two different temporal scales: the 24 h mean values allowed comparison with $PM_{2.5}$ and trace elements measurements, and subsequent SEM-EDX analysis. Higher temporal resolution (1 h) measurements were useful to improve the assessment, when present, of the rapid variations in COVA emissions often characterized by short and intense peaks (Calvello et al., 2015, 2014).

4. Observations and discussion

To obtain potential day-by-day concentration variations, an overview of 24 h means for the main measured in-situ and meteorological parameters is reported in Table 1.

$PM_{2.5}$ daily mass concentration observed in the Agri Valley during the IMAA campaign ranged between 2.2 μg m^{-3} and 8.8 μg m^{-3} with a mean value of 5.0 ± 2.4 μg m^{-3} over the entire period.

The minimum of $PM_{2.5}$ was registered on July 3 together with maximum values of EBC, NO_2, SO_2, CH_4, NMHC and CO.

Measured $PM_{2.5}$ mass concentrations are comparable with values measured in rural and background sites (Contini et al., 2014; Hueglin et al., 2005) and generally lower than those observed in other industrial or urban areas (Cesari et al., 2016; Sudheer and Rengarajan, 2012).

EBC values are higher than both mean values observed during July and September in 2013 (545 ± 324 ng/m^3) and mean values (568 ± 362 ng/m^3) for 2013 (Calvello et al., 2015). EBC concentrations measured during the IMAA campaign are also higher than 500 ng/m^3, measured at an industrial site (oil and gas activities) in a rural area in Texas, over a 20 day period in June 2011 (Rutter et al., 2015).

In general, mean values of gaseous compounds are lower than mean values found between September and October in 2013 at the site (Calvello et al., 2014), probably related to a higher mixing height. However, in relation to SO_2, measured concentrations are comparable or even higher than those from long-term datasets from traffic, urban background and industrial sites in Europe as reported in Karanasiou et al. (2014) and Reche et al. (2011). These relevant SO_2 concentrations agree with Semeniuk et al. (2015) at the Habshan industrial site in United Arab Emirates, where oil and gas processing represents the main source of pollution at a regional-scale, and for Bari and Kindzierski (2017) for the Red Deer county in Canada which hosts oil and gas industries.

Regarding the aerosol columnar optical properties, a summary of the radiometric data i.e spectral AOD, alpha exponent and inverted size distribution for July 3, 16 and 17 is reported in Fig. S1 of the supplementary material. The obtained AODs were used as the input data for the radiometric model described in Section 3 and in Pavese et al. (2016) to evaluate the contribution of the modeled aerosol components compared with the measured columnar AODs. In particular, considering the characteristics of the measurement site, the following 8 components were considered suitable in describing the aerosol loading: water soluble (WS), black carbon (BC), sea salt coarse mode (SScoa), sea salt accumulation mode (SSacc), mineral transported (MT), mineral nucleation (Mnuc), mineral coarse (Mcoa) and biogenic (Bio). As reported in Pavese et al. (2016), WS and BC components generally prevail in polluted conditions, well representing the fine anthropogenic fraction of aerosols. Apart from cases in marine or desert sites, sea-salt and

Table 1
Mean daily concentrations of atmospheric and meteorological parameters with corresponding standard deviations.

Parameter	07/02	07/03	07/11	07/12	07/13	07/14	07/15	07/16	07/17
$PM_{2.5}$ (μg/Nm^3)	5.3	2.2	8.8	3.6	3.4	2.9	7.9	3.3	7.2
EBC (ng/m^3)	667 ± 245	956 ± 252	747 ± 179	820 ± 334	818 ± 231	851 ± 338	838 ± 614	674 ± 131	663 ± 209
SO_2 (μg/m^3)	6.8 ± 3.4	9.6 ± 4.6	5.7 ± 3.3	4.5 ± 2.1	8.4 ± 6.7	4.4 ± 0.7	4.8 ± 1.0	5.9 ± 3.6	4.8 ± 1.6
NO_2 (μg/m^3)	10.7 ± 8.0	18.2 ± 14.7	12.4 ± 12.8	8.1 ± 2.5	11.6 ± 9.2	7.2 ± 1.4	8.1 ± 2.5	8.4 ± 4.2	6.6 ± 1.3
CO (mg/m^3)	0.25 ± 0.01	0.28 ± 0.02	0.25 ± 0.01	0.25 ± 0.04	0.25 ± 0.02	0.25 ± 0.01	0.24 ± 0.01	0.25 ± 0.02	0.23 ± 0.01
C_6H_6 (μg/m^3)	0.65 ± 0.13	0.83 ± 0.31	0.82 ± 0.14	0.90 ± 0.42	0.90 ± 0.23	0.90 ± 0.14	0.78 ± 0.16	0.96 ± 0.31	0.82 ± 0.13
toluene (μg/m^3)	0.37 ± 0.14	0.60 ± 0.31	0.66 ± 0.21	0.99 ± 1.29	0.76 ± 0.30	0.71 ± 0.34	0.48 ± 0.13	0.58 ± 0.32	0.43 ± 0.16
CH_4(μgC/m^3)	926 ± 44	934 ± 55	918 ± 46	918 ± 38	931 ± 53	933 ± 65			
NMHC(μgC/m^3)	59.7 ± 38.3	124.2 ± 160.1	67.8 ± 12.6	73.5 ± 31.5	74.8 ± 35.7	64.8 ± 9.8			
H_2S (μg/m^3)	1.6 ± 0.4	1.8 ± 0.4	1.7 ± 0.4	1.7 ± 0.4	2.1 ± 1.1	1.7 ± 0.5	1.7 ± 0.4	1.9 ± 0.4	1.6 ± 0.4
T (°C)	20 ± 6	21 ± 6	19 ± 4	20 ± 5	21 ± 6	20 ± 3	21 ± 5	21 ± 6	20 ± 6
RH (%)	55 ± 19	61 ± 18	83 ± 14	80 ± 18	74 ± 21	83 ± 13	70 ± 20	57 ± 18	59 ± 18
P (mBar)	946 ± 1	945 ± 1	942 ± 1	945 ± 1	946 ± 1	946 ± 1	946 ± 1	947 ± 1	947 ± 1
GR (W/m^2)	286 ± 351	281 ± 344	201 ± 244	262 ± 358	282 ± 341	157 ± 211	267 ± 340	271 ± 352	302 ± 373
ws (m/s)	1.17 ± 0.70	1.51 ± 1.02	0.94 ± 0.56	1.08 ± 0.91	1.07 ± 0.81	0.84 ± 0.60	0.88 ± 0.30	1.35 ± 0.68	1.39 ± 0.55
rain (mm)	0.11	0.17	1.8	0.16	0.00	0.10	0.01	0.00	0.01

mineral components account for transported aerosols from the sea or from desert areas respectively, even if a part of mineral component can also be associated with re-suspended dust. Anthropogenic emissions from COVA were expected to mainly influence the aerosol loading at the site and the radiometric model results, reported in pie-plots in Fig. 2, are consistent with this hypothesis. In fact, a similar composition was obtained for both July 3 and 16, with the maximum contribution of the fine anthropogenic aerosols (BC + WS accounting for 52%–57%). The traffic from heavy vehicles in related to COVA activities and the presence of many unpaved roads in the vicinity of the plant was assumed to represent a source of coarse mineral particles, verified by the presence of a relevant contribution of Mcoa to the total AOD (about 24%). Hysplit trajectories calculated for July 3, 16 and 17 (Fig. S2 of the supplementary material) allowed verification that for July 17 most airmasses originated over the Atlantic Ocean in agreement with a more heterogeneous situation described by model results (Fig. 2). In fact in this case a non negligible contribution of sea-salts particles (fine and coarse accounting for about 32%) was found.

With regards to biogenic aerosols component, a similar contribution (from about 10% to 15%) was found for all three days, probably due to the summer season.

4.1. Trace elemental $PM_{2.5}$ composition

Table 2 shows the mean concentrations of the 17 trace elements measured in $PM_{2.5}$ aerosol particles at the site. The most abundant trace elements were S, Ca, Fe, Na, K and Mg with average concentrations ranging from 100 to 700 ng m^{-3}. Moderate abundances were obtained for Al and Zn (87 and 80 ng m^{-3}, respectively) followed by Li, P, Cr, Ti, Mn and Cu with concentrations ranging from 10 to 100 ng m^{-3}. Finally, the trace elements with concentrations less than 5 ng m^{-3} were Pb, Ni and Cd.

Compared with data reported in literature, mean concentration of Ca is higher than those found at other suburban/rural and rural background (Schwarz et al., 2016) sites or other industrial/urban sites. Al shows mean concentration values similar to those measured in a highly industrialized chemical/petrochemical area (Paulino et al., 2014). Atmospheric mean concentrations of Fe, Cu, Ni, Mn, Zn, Cr and Ti are significantly higher if compared to the values from other urban/industrial sites (Contini et al., 2014; Paulino et al., 2014), but lower if compared with mean values observed in polluted sites (Chen et al., 2015). Cd, K, Li, Mg, Na and S mean concentrations show comparable or lower values than those reported at industrial and sub-urban sites (Hieu and Lee, 2010; Vecchi et al., 2004).

As far as Pb concentration is concerned, similar concentrations of a background area were found (Schwarz et al., 2016), lower than those measured on industrial and urban sites (Contini et al., 2014; Sudheer and Rengarajan, 2012).

Table 2
Mean, standard deviation, minimum and maximum values of concentrations (expressed in ng/m^3) of the 17 measured trace elements.

Element	Mean	St.Dev	Min	Max
S	703,1	1054,9	60,8	3379,1
Ca	657,1	423,0	178,9	1187,7
Fe	335,0	285,9	91,1	827,8
Na	177,1	67,1	111,4	307,4
K	166,0	50,9	117,1	246,9
Mg	107,4	27,8	67,2	150,1
Al	87,8	60,7	42,4	210,7
Zn	80,1	68,5	15,1	245,2
Li	37,4	5,4	28,8	45,2
P	36,5	14,9	20,1	70,5
Cr	24,8	5,9	16,0	34,8
Ti	22,3	8,4	10,7	38,1
Mn	14,4	10,4	4,0	33,2
Cu	13,2	8,6	2,9	27,8
Pb	4,3	2,5	0,8	9,0
Ni	4,0	2,5	1,4	8,9
Cd	0,9	1,3	0,0	4,0

In order to gain a better understanding of the correlation structure between the measured trace element concentrations, Pearson's correlation coefficients (ρ) are reported in Table 3, as a high correlation coefficient between two trace elements could mean a common source. The more significant correlations (ρ > 0.80) are indicated in bold and relate to Al-Na, Na-K, Zn-S, Zn-Ni.

The correlation Al-Na (ρ = 0.85) is generally due to a natural source mainly related to crustal material and natural long-range transport. In this area, behind the natural source of these elements, this significant correlation could be explained by a common local anthropogenic source, mainly related to oil desulfurization by means of NaOH and $NaHCO_3$, and sulfur liquefaction (Al_2O_3 used as a catalyst) by the COVA industrial process (EU-JRC-IPTS, 2015). In fact, even if it is not mentioned in any ENI document regarding the COVA plant, as described in EU-JRC-IPTS (2015), the LABSORB regenerative process is based on an absorption/regeneration cycle including the use of an absorbing solution containing caustic soda and phosphoric acid to capture SO_2 as sodiumbisulphite.

A high correlation of K was found with Na (ρ = 0.87), which could be due to both anthropogenic sources of K related to combustion processes and to natural sources.

The significant correlation between Zn-S and Zn-Ni is interesting, Zn and Ni are present in high concentrations in the study area and are commonly considered tracers of industrial process. In particular, Ni is a tracer of oil-burning and/or oil refining industries (Celo and Dabek-Zlotorzynsk, 2010). Their correlation, therefore, together with a good correlation between S-Zn could suggest a common anthropogenic/industrial origin.

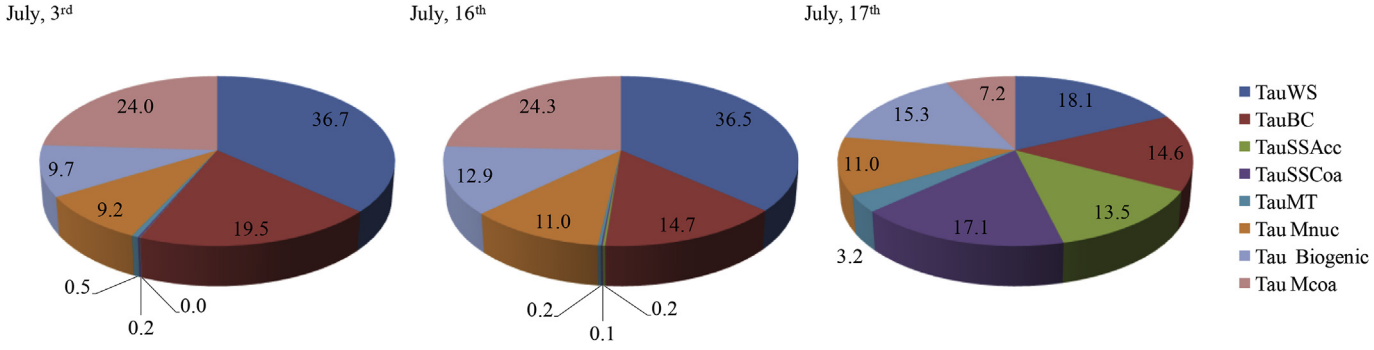

Fig. 2. Model-estimated columnar aerosol percentage compositions for July 3, 16 and 17. Each AOD component is affected on average by a 10% error (experimental and statistical).

Table 3
Pearson correlation coefficients calculated for the 17 measured trace elements and $PM_{2.5}$.

	Al	Ca	Cd	Cr	Cu	Fe	K	Li	Mg	Mn	Na	Ni	P	Pb	S	Ti	Zn	$PM_{2.5}$
Al	1,00	0,16	0,36	0,14	0,17	0,38	0,59	0,47	0,02	0,03	**0,85**	0,04	0,09	0,34	0,03	0,22	0,09	−0,06
Ca		1,00	0,43	0,74	0,59	0,12	0,19	0,16	0,21	0,11	0,10	0,42	0,47	0,68	0,21	0,06	0,14	0,34
Cd			1,00	0,14	0,12	0,62	0,05	0,45	0,55	0,32	0,33	0,28	0,43	0,58	0,24	0,30	0,10	0,27
Cr				1,00	0,77	0,43	0,13	0,16	0,67	0,27	0,20	0,21	0,11	0,24	0,09	0,43	0,21	0,00
Cu					1,00	0,29	0,42	0,31	0,59	0,42	0,40	0,53	0,39	0,49	0,34	0,59	0,17	0,29
Fe						1,00	0,32	0,35	0,69	0,56	0,28	0,17	0,20	0,64	0,32	0,59	0,03	0,04
K							1,00	0,01	0,37	0,35	**0,87**	0,74	0,17	0,60	0,45	0,02	0,53	0,38
Li								1,00	0,22	0,55	0,29	0,30	0,12	0,13	0,01	0,05	0,40	0,20
Mg									1,00	0,14	0,33	0,26	0,34	0,08	0,36	0,65	0,17	0,25
Mn										1,00	0,24	0,11	0,53	0,19	0,26	0,28	0,18	−0,13
Na											1,00	0,38	0,25	0,47	0,17	0,09	0,14	0,03
Ni												1,00	0,26	0,61	0,68	0,13	**0,81**	0,60
P													1,00	0,48	0,10	0,16	0,06	−0,38
Pb														1,00	0,03	0,07	0,16	0,48
S															1,00	0,35	**0,87**	0,51
Ti																1,00	0,24	−0,28
Zn																	1,00	0,50
$PM_{2.5}$																		1,00

Values in bold indicate the significant correlations.

4.2. SEM-EDX results

Based on both morphology and chemical composition, particles collected during the IMAA campaign were grouped into Silicates, Ca-bearing, Metal, Fly ash, S-rich, Silica and Silicate mixture particles as reported in Table 4. Carbonaceous particles were not counted in this analysis due to the interference with both Carbon in graphite filters coating and Carbon within polycarbonate filters, however morphological and chemical analysis was performed on these particles.

In order to estimate the error associated with the particles classification, a cross check procedure was carried out according to Semeniuk et al. (2015) and our previous experience (Lettino et al., 2017; Pavese et al., 2016). In fact, particles were checked for both morphologies and EDX spectra, obtaining an estimated error <1% for their attribution to the different families. For this reason, families with particle number percentages less than 1% were not considered in this study, apart from fly ash due to both their spherical morphology and typical composition allowing an easier and unequivocal classification.

At very first glance, peculiar morphologies at this site, particularly for Silicates, Ca-bearing, Silica and Silicates mixtures were highlighted. Silicates can have an irregular shape or the usual lamellar morphology of clay minerals (Fig. 3a) and can sometimes be found as slag particles with a rough surface texture (Fig. 3b) (Latifi et al., 2015; Xie et al., 2005). They are composed by Si and Al, mainly associated with Fe and K and subordinately to Ca and Mg. Less often, silicates are found with Si-Fe and/or Ca and/or Mg only. S is frequently found in Silicates composition due to heterogeneous reactions that have likely taken place over particles surfaces.

Silicates found were abundant for all measurement days, with number percentages varying from the minimum value of 21% on July 11 to the maximum value of 42% on July 16. The lower values were mostly associated with a decrease in the coarse fraction (D > 1 μm).

The most frequent compositions of Ca-bearing particles were Ca-Al-Na or Ca-Mg, rarely Ca-only. Small quantities of Fe and/or P could enter into the particles composition. Morphology and dimension allow for the discrimination between different Ca-bearing particles. Ca-Al-Na particles, mostly <1 μm, showed rough surfaces and signs of cracks, (Fig. 3c), Ca-only particles, < 1 μm, were irregularly shaped and with soluble phases on their surfaces. Ca-Mg particles were greater than 1 μm and show squat or irregular shape with smooth surfaces (Fig. 3d). Ca-bearing particles number percentages varied in the 5–19% range with higher values on July 2 and mainly due to an increase in the Ca-Mg fraction.

Metals oxides/hydroxides were irregularly shaped (Fig. 3e), sometimes as spherical particles (Fig. 3f), generally less than 1 μm sized. Fe is the main component with some S and Si traces. Zn is also quite often associated with Fe and/or S and/or Na, and characterizes the chemical composition as previously assessed by chemical analysis, whereas metallic Fe phases associated with Cu, Cr, Ni, Pb, are more rare. Metal oxides/hydroxides represent approximately between 20% and 30% of the total number of particles.

The typical spherical shape characterizes fly ashes with a chemical composition mostly attributable to Si-Al-K-Fe ± Mg, +/− Ca. They are sometimes found as particles with localized Na-sulfates salts on the surface (Fig. 3g). Generally fly ash contribution to the total number of particles is low (~1%) with higher values on July 11 (3.1%) and 12 (2.6%). This increase could be due to long-range transport contribution. In fact, the low-level HYSPLIT airmass

Table 4
Classification criteria of different particle groups and their number percentage for each sampling day.

Particle groups	Major selection criteria Chemical[a] and Morphological	07/02	07/03	07/11	07/12	07/13	07/14	07/15	07/16	07/17
Silicate	Si + Al > 60%	23.6	27.8	21.0	40.7	36.7	36.5	39.0	42.0	33.0
Ca_bearing	Ca + Mg>90% sometime with minor Fe or P or Na	19.3	11.0	8.5	4.8	8.6	4.8	6.0	6.0	9.5
Metal	Metals (Fe, Zn, Al, Mn, Cu, Ti) > 80%	27.0	23.2	22.3	27.8	24.9	21.6	34.1	28.0	26.2
S-rich	S>30% and (Ca and/or Mg and/or Al and/or Na) > 40%	22.3	29.5	32.6	16.5	14.5	26.0	10.9	11.2	18.6
Silice	Si>85%	5.6	5.1	7.6	3.3	10.9	6.3	4.9	8.0	8.6
Fly ash	Si + Al > 60% and spherical	0.9	0.0	3.1	2.6	1.4	0.5	0.7	1.2	1.4
Silicate mixtures	Mixtures of silicate and another particle groups	1.3	3.4	4.9	4.4	3.2	4.3	4.5	3.6	2.7

[a] X-ray intensities of elements relative to the sum of net counts of elements with Z > 10.

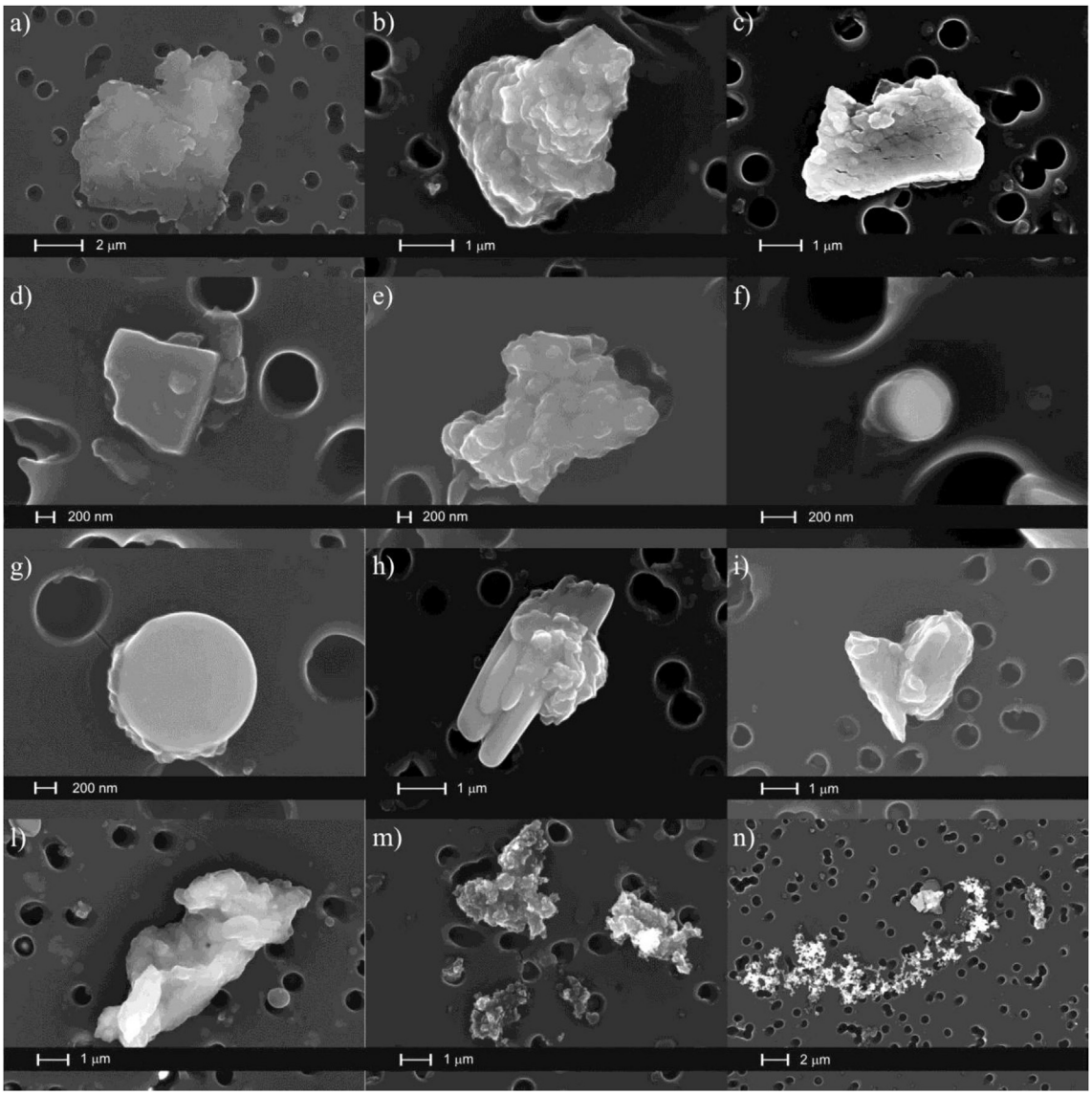

Fig. 3. SEM photomicrographs of airborne particles sampled on the polycarbonate filter in the Agri Valley. (a) phyllosilicates (clay minerals), (b) agglomerate of small silicate particles (slag), (c) aggregate phases mainly composed of Ca with Na and Al, (d) Ca-Mg carbonate (dolomite), (e) Iron particle, (f) Fe-Zn particle, (g) fly ash particle with Na-sulfates on the surface, (h) aggregate crystal of Ca-Na-sulfates, (i) soil derived quartz, (l) Beam-damaged non-mineral particle mainly composed of Si (amorphous silica), (m) embedded soot, (n) fresh soot aggregate.

moves very close to the ground in Northern-Eastern Europe before its arrival at the measurement site (Fig. S3 of the supplementary material).

S-rich particles were mostly found as Ca and Na sulfate particles and, subordinately, as S-only or S-Na particles. Occasionally S-K crystals with dimensions of <1 μm and, sometimes, > 1 μm were observed. In particular, Ca-Na-S particles were found as heterogeneous phases of Ca-S aggregated elongated crystals with Na-S formations on their surface (Fig. 3h). S-only particles were found in the finer fraction as droplets (H_2SO_4), whereas S-Na particles could be partially or totally reacted H_2SO_4 aerosol giving $(NH_4)_2SO_4$ or Na_2SO_4. S-rich particle number percentages varied from 11% to 33% with higher values on July 3, 11 and 14. On July 11, 14 and 17 an increased contribution of the S-only group was observed.

Silica particles can vary in size, with morphologies of natural quartz (squat particles and smooth surfaces, Fig. 3i) or they can be irregularly shaped with rough surfaces. In this case, they can have a melted aspect or can be easily beam-damaged suggesting an amorphous phase or the presence of soluble phases on their surface (Fig. 3l). As well as for silicates, coarser Silica particle fractions were minimum on July 11.

Silicates mixtures were mainly composed of Si, S and Ca, with minor contributions of Al, Mg, K and Fe and, for this reason, are classified as mixed particles (gypsum/silicate and/or Ca-Mg-carbonates).

Carbonaceous particles, including biogenic (fungal spores and biogenic fragments), organic particles and soot also contribute to the aerosol composition and as previously mentioned, were not counted. However morphological analyses were performed on soot particles in particular and were generally found as 1–3 μm sized embedded clusters (aged soot, Fig. 3m), and particularly less frequently as spherules chains on July (fresh soot, Fig. 3n). The presence of S-coating was often detected by EDX spectra.

Table 5
Central diameters of the 16 OPS channels.

Bins	1	2	3	4	5	6	7	8	9	10	11	12	13	14	15	16
D (μm)	0.34	0.42	0.52	0.65	0.81	1.0	1.2	1.6	1.9	2.4	3.0	3.7	4.7	5.8	7.2	9.0

4.3. EBC, OPS and gaseous compound measurements

Throughout each measurement day a very low variability was observed for OPS 1-hourly averaged size distributions, each of them were well represented by the 24 h averaged distribution (Fig. S4 of the supplementary material). To compare OPS data to both EBC and gaseous compound data on the higher resolution temporal scale of 1 h, different OPS channels (central diameters for each OPS channel are reported in Table 5) were considered separately to observe the variations of temporal patterns. In addition, daily correlation coefficients between the different atmospheric components and OPS channels were calculated.

The contribution of the atmospheric components compared to the total number of particles counted by OPS changes on a day-by-day basis as shown in Fig. 4 where, as an example, temporal trends of hourly averaged OPS counts for channel 1 (OPS_1 hereafter) together with EBC and some gaseous compounds averaged hourly concentrations are reported. OPS_1 is considered as representative of the finest fraction of the size distribution that was verified to be more influenced by both EBC and gaseous compounds (CH_4, NO_2 and SO_2) concentration variability.

Due to the typical dimensions of fresh emitted EBC (Bond et al., 2013; Lack et al., 2014) and to the strong vicinity of the measurement site to COVA, a relevant contribution of fresh EBC to the fine particles loading at the site was expected. The similar temporal patterns of EBC and OPS_1 for all measurement days (Fig. 4a) are consistent with this hypothesis. In particular, during the early morning of July 15th (Fig. 4a), a process mostly involving BC particles can be assumed to have occurred due to the presence of the intense simultaneous peak for EBC and OPS_1 only, registered at 5.25 a.m. GMT. The highest values of correlation coefficients calculated among between EBC and OPS channels were recorded on July 14 with R^2 ranging from 0.77 to 0.91 for the first four OPS channels.

Based on previous studies by Calvello et al. (2014, 2015) for the same site, an overall concurrence between EBC and CH_4 temporal trends was expected. The CH_4 and the EBC morning concentration peaks coincided for most of the measurement days agreeing with the previous findings. As shown in Fig. 4b, the recurrent CH_4 peaks during the morning hours play a role in the fine particle load increase particularly on July 14 when, as for EBC, a good correlation was found among the first three OPS channels ($0.34\ \mu m < D < 0.65\ \mu m$) and CH_4 with R^2 ranging from 0.65 to 0.71. Simultaneous emissions of fresh BC particles and CH_4 molecules could be inferred on this day based on the concurrence between EBC and CH_4 ($R^2 = 0.7$).

The well-known role of NO_2 and SO_2 as precursors in the formation of secondary aerosols (Indarto, 2012) could explain the coincidence of their concentration peaks with OPS1 peaks as in Fig. 4c and d. In fact, the 1 h averaging period was thought to be enough for NO_2 and SO_2 to become acids with the typical time of reaction of $4.3 \times 10^{-3}\ s^{-1}$ (Indarto, 2012) and then participate to the gas-particle partitioning.

4.4. Integrating SEM-EDX observations and chemical analysis

Beginning with the integration of SEM-EDX observations and $PM_{2.5}$ chemical analysis, attention was focused on some processes occurring at COVA, or strictly related to COVA activities as the erosion of the plant pipelines or the traffic from heavy vehicles, thought to be responsible for the distinctive features in the observed particles. In addition, the possible influence of RH on the formation of particles was examined exploiting the useful indications obtained by this integrated approach.

The common use of powders containing Ca, Al and Na ($CaCO_3$, CaO, $Ca(OH)_2$, Al_2O_3, NaOH, $NaHCO_3$) in desulfurization and sulfur liquefaction processes, was supposed to be the main source of Ca-Na-Al particles detected by SEM-EDX analysis, especially in the fine fraction of all samples. Their peculiar morphology, different from the typical natural crustal morphology of Ca-Mg-carbonates, is characterized by rough surfaces and signs of cracks, probably produced by the above-cited anthropogenic processes that could have also lead to the production of Ca-S and Ca-S-Na particles found on filters. The chemical analysis described above are consistent with this hypothesis thanks to the relevant correlation between Na and Al (Table 3).

The continuous plant pipeline erosion, a source of emissions independent from COVA activities, is expected to be related to the poor day-by-day variability in metals oxides/hydroxides composition with Fe, Zn and Al as the prevailing elements, found using both chemical analysis and SEM observations.

The observations on Sunday 14 July showed a strong decrease in Ca-Mg particles number percentage contribution compared to other days and this result is consistent with the re-suspension from unpaved road as the main source of Ca-Mg particles emission probably due to the influence of heavy traffic in the vicinity.

The role of RH in the modification of the efficiency in gas to particle conversion processes, especially for S-compounds, was investigated starting from the variability of RH values (Table 1).

Low values of RH (61%) on July 3, corresponded with a minimum of $PM_{2.5}$ together with maximum concentrations of most gaseous compounds and a low amount of S-only particles detected by SEM-EDX, being consistent with a reduction in gas-to particle conversion. This was strengthened by the results from July 11 when $PM_{2.5}$ and S mass concentrations were maximum, the S-only particles contribution increased due to higher RH values (83%), even though SO_2 concentrations were lower (Table 1). An intermediate situation was observed on July 14 when lower SO_2 emissions and the same RH compared with July 11, corresponded with lower S mass concentration.

5. Conclusions

A multi-instrumental approach allowed the ample characterization of aerosol loading at the COVA site in the Agri Valley during the short-term IMAA campaign. This was the first attempt to integrate different measurement techniques in such a unique site to better assess aerosol chemical, morphological and optical properties and to obtain information on mixing effects and transformation processes also related to meteorological parameters. Chemical analysis on $PM_{2.5}$ filters provided a picture of relative abundances of different elements highlighting the role of S, Zn and Ni as markers of COVA activities. SEM morphological observations enriched the description with the main families of particles detected at the site, allowing for the identification of anthropogenic origin of many silicates likely modified by extraction processes or by Ca-Al-Na particles from desulfurization and sulfur liquefaction

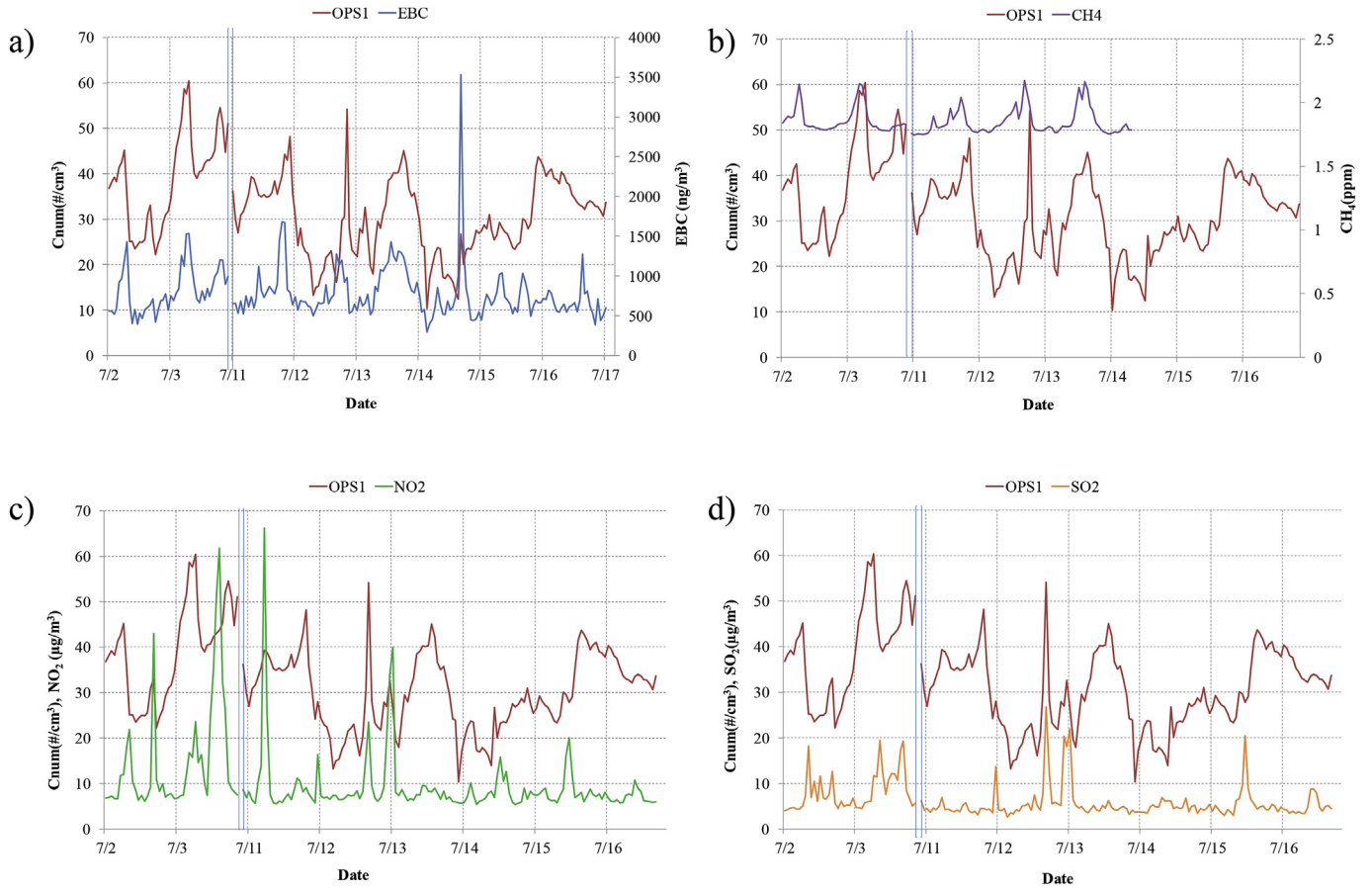

Fig. 4. Temporal patterns of hourly concentrations of a) OPS_1 and EBC, b) OPS_1 and CH_4, c) OPS_1 and NO_2, d) OPS_1 and SO_2. The blue vertical lines indicate the period of measurement stops. (For interpretation of the references to colour in this figure legend, the reader is referred to the web version of this article.)

processes. The simultaneous use of an OPS, an aethalometer and the availability of gaseous concentration data allowed for the verification of the key role of gaseous emissions, typical of oil processing such as SO_2 and CH_4, in formation processes of particles. EBC concentrations were found to significantly contribute to the total number of fine particles measured by OPS (fresh BC). The ability to compare $PM_{2.5}$ mass data, SEM-EDX observations and meteorological parameters provided information on gas-to-particle conversion mechanisms strongly influenced by RH.

The comparison among in-situ and columnar observations allowed for the evaluation of and to which extent aerosol loading in the lower layers influences the upper layers. On July 3, the concurrent higher concentration values for EBC and for most of the gaseous compounds at ground level, concurred with the maximum contribution of the fine mode anthropogenic aerosols (BC + WS) estimated over the atmospheric column.

Based on the results, the integrated approach used in this study can contribute to improve the assessment of the impact of industrial emissions from COVA on air quality in the Agri Valley, representing a key element in planning pollution control management policies. In addition, this kind of study can be reproduced at similar sites, where attention is generally focused on gaseous compounds, thus giving a more complete picture which includes information on the aerosol fraction.

Acknowledgments

This study was partially supported by the Smart Basilicata project (PON 04A200165), funded by the Italian Ministry of Education, University and Research and by the 2007–2013 Basilicata Regional Authority Cohesion Fund.

Appendix A. Supplementary data

Supplementary data related to this article can be found at https://doi.org/10.1016/j.atmosenv.2017.09.026.

References

Andreae, M.O., Jones, C.D., Cox, P.M., 2005. Strong present-day aerosol cooling implies a hot future. Nature 435, 1187–1190.
Baltrėnas, P., Baltrėnaitė, E., Šerevičienė, V., Pereira, P., 2011. Atmospheric BTEX concentrations in the vicinity of the crude oil refinery of the Baltic region. Environ. Monit. Asses. 182, 115–127.
Bari, MdA., Kindzierski, W.B., 2017. Characteristics of air quality and sources affecting fine particulate matter ($PM_{2.5}$) levels in the City of Red Deer, Canada. Environ. Pollut. 221, 367–376. https://doi.org/10.1016/j.envpol.2016.11.087.
Bond, T.C., Doherty, S.J., Fahey, D.W., Forster, P.M., Berntsen, T., DeAngelo, B.J., Flanner, M.G., Ghan, S., Kärcher, B., Koch, D., Kinne, S., Kondo, Y., Quinn, P.K., Sarofim, M.C., Schultz, M.G., Schulz, M., Venkataraman, C., Zhang, H., Zhang, S., Bellouin, N., Guttikunda, S.K., Hopke, P.K., Jacobson, M.Z., Kaiser, J.W., Klimont, Z., Lohmann, U., Schwarz, J.P., Shindell, D., Storelvmo, T., Warren, S.G., Zender, C.S., 2013. Bounding the role of black carbon in the climate system: a scientific assessment. J. Geophys. Res. 118, 5380–5552.
Caggiano, R., D'Emilio, M., Macchiato, M., Ragosta, M., 2001. Experimental and statistical investigation on atmospheric heavy metal concentrations in an industrial area of Southern Italy. Nuovo Cimento C 24, 391–406.
Calvello, M., Esposito, F., Trippetta, S., 2014. An integrated approach for the evaluation of technological hazard impacts on air quality: the case of the Val d'Agri oil/gas plant. Nat. Hazards Earth Syst. Sci. 14, 2133–2144.
Calvello, M., Esposito, F., Lorusso, M., Pavese, G., 2015. A two-year database of BC measurements at the biggest European crude oil pre-treatment plant: a

comparison with organic gaseous compounds and PM_{10} loading. Atmos. Res. 164–165, 156–166.
Celo, V., Dabek-Zlotorzynsk, E., 2010. Concentration and source origin of trace metals in $PM_{2.5}$ collected at selected canadian sites within the canadian national air pollution surveillance program. In: Zereini, F., Wiseman, C.L.S. (Eds.), Urban Airborne Particulate Matter, Environmental Science and Engineering. DOI: 10.1007/978-3-642-12278-1_2.
Cesari, D., Donateo, A., Conte, M., Merico, E., Giangreco, A., Giangreco, F., Contini, D., 2016. An inter-comparison of $PM_{2.5}$ at urban and urban background sites. Atmos. Res. 174–175, 106–119.
Chen, Y., Hsu, C., Lin, S., Chang-Chien, G., Chen, M., Fang, G., Chiang, H., 2015. Characteristics of concentrations and metal compositions for PM2.5 and $PM_{2.5-10}$ in Yunlin county. Taiwan Dur. Air Qual. Deterioration Aerosol Air Qual. Res. 15, 2571–2583.
Cheng, T., Wu, Y., Gu, X., Chen, H., 2015. Effects of mixing states on the multiple scattering properties of soot aerosols. Opt. Express 23, 8. https://doi.org/10.1364/OE.23.010808.
Contini, D., Cesari, D., Donateo, A., Chirizzi, D., Belosi, F., 2014. Characterization of PM_{10} and $PM_{2.5}$ and their metals content in different typologies of sites in south-eastern Italy. Atmosphere 5, 435–453. https://doi.org/10.3390/atmos5020435.
Dockery, D.W., 2001. Epidemiologic evidence of cardiovascular effects of particulate air pollution. Environ. Health Perspect. 109, 483–486.
Draxler, R.R., Rolph, G.D., 2003. HYSPLIT (Hybrid Single-particle Lagrangian Integrated Trajectory) Model. NOAA Air Resour. Lab., Silver Spring, MD. http://ready.arl.noaa.gov/HYSPLIT.php. last access January 2017.
ENI (Ente Nazionale Idrocarburi), 2014. ENI in Basilicata, Local Report 2014 available at: https://www.eni.com/eni-basilicata/files/documenti/local-report-2014.pdf. in Italian, last access January 2017.
EU-JRC-IPTS (European Commission - Joint Research Centre Institute for Prospective Technological Studies), 2015. Best Available Techniques (BAT) Reference Document for the Refining of Mineral Oil and Gas. Industrial Emissions Directive 2010/75/EU. Report EUR 27140 EN, available at: http://eippcb.jrc.ec.europa.eu/reference/BREF/REF_BREF_2015.pdf. last access January 2017.
Fawole, O.G., Cai, X.-M., MacKenzie, A.R., 2016. Gas flaring and resultant air pollution: a review focusing on black carbon. Environ. Pollut. 216, 182–197.
Hansen, A.D.A., 2005. The Aethalometer Manual, Magee Scientific available at: https://www.psi.ch/catcos/ProjectDetailCatcosOperationsEN/Aethalometer_book_2005.07.02.pdf. Last access: March 2017.
Hieu, N., Lee, B., 2010. Characteristics of particulate matter and metals in the ambient air from a residential area in the largest industrial city in Korea. Atmos. Res. 98, 526–537.
Hueglin, C., Gehrig, R., Baltensperger, U., Gysel, M., Monn, C., Vonmon, H., 2005. Chemical characterization of $PM_{2.5}$, PM_{10} and coarse particles at urban, near-city and rural sites in Switzerland. Atmos. Environ. 39, 637–651.
Indarto, A., 2012. Heterogeneous reactions of HONO formation from NO2 and HNO3 : a review. Res. Chem. Intermed. 38, 1029–1041. https://doi.org/10.1007/s11164-011-0439-z.
Jacobson, M.Z., Streets, D.G., 2009. The influence of future anthropogenic emissions on climate, natural emissions and air quality. J. Geophys. Res. 114, D08118.
Karanasiou, A., Querol, X., Alastuey, A., Perez, N., Pey, J., Perrino, C., Berti, G., Gandini, M., Poluzzi, V., Ferrari, S., de la Rosa, J., Pascal, M., Samoli, E., Kelessis, A., Sunyer, J., Alessandrini, E., Stafoggia, M., Forastiere, F., the MED-PARTICLES Study Group, 2014. Particulate matter and gaseous pollutants in the Mediterranean Basin: results from the MED-PARTICLES project. Sci. Total Environ. 488–489, 297–315.
Koch, D., Del Genio, A.D., 2010. Black carbon semi-direct effects on cloud cover: review and synthesis. Atmos. Chem. Phys. 10, 7685–7696.
Künzi, L., Mertes, P., Schneider, S., Jeannet, N., Menzi, C., Dommen, J., Baltensperger, U., Prévôt, A.S.H., Salathe, M., Kalberer, M., Geiser, M., 2013. Responses of lung cells to realistic exposure of primary and aged carbonaceous aerosols. Atmos. Environ. 68, 143–150.
Lack, D.A., Mosmüller, H., McMeeking, G.R., Chakrabarty, R.K., Baumgardner, D., 2014. Characterizing elemental, equivalent black, and refractory black carbon aerosol particles: a review of techniques, their limitations and uncertainties. Anal. Bioanal. Chem. 406, 99–122. https://doi.org/10.1007/s00216-013-7402-3.
Latifi, N., Marto, A., Rashid, A.S.A., Yii, J.L.J., 2015. Strength and physico-chemical characteristics of fly ash-bottom ash mixture. Arabian J. Sci. Eng. 40 (9), 2447–2455.
Lettino, A., Calvello, M., Esposito, F., Fiore, S., Lorusso, M., Pavese, G., 2017. Effects of polluted air-masses advection on atmospheric particles in a semi-rural site in south Italy by SEM-EDX analysis. Aerosol Air Qual. Res. 17, 69–83.
Lin, T.-Y., Sree, U., Tseng, S.-H., Chiu, K.H., Wu, C.-H., Lo, J.-G., 2004. Volatile organic compound concentrations in ambient air of Kaohsiung petroleum refinery in Taiwan. Atmos. Environ. 38, 4111–4122.
Lopes Oliveira, R., Varandas, L., Arbilla, G., 2014. Characterization of polycyclic aromatic hydrocarbon levels in the vicinity of a petrochemical complex located in a densely populated area of the Rio de Janeiro, Brazil. Atmos. Pollut. Res. 5, 87–95.
Margiotta, S., Lettino, A., Speranza, A., Summa, V., 2015. PM1 geochemical and mineralogical characterization using SEM-EDX to identify particle origin – Agri Valley pilot area (Basilicata, southern Italy). Nat. Hazards Earth Syst. Sci. 15, 1551–1561. https://doi.org/10.5194/nhess-15-1551-2015.
Morawska, L., Zhang, J., 2002. Combustion sources of particles. 1. Health relevance and source signatures. Chemosphere 49 (9), 1045–1058.
Pavese, G., Calvello, M., Esposito, F., 2012. Black Carbon and organic components in the atmosphere of Southern Italy: comparing emissions from different sources and production processes of carbonaceous particles. Aerosol Air Qual. Res. 12, 1146–1156.
Pavese, G., Lettino, A., Calvello, M., Esposito, F., Fiore, S., 2016. Aerosol composition and properties variation at the ground and over the column under different air masses advection in South Italy. Environ. Sci. Pollut. Res. 23, 6546–6562.
Paulino, S.A., Oliveira, R.L., Loyola, J., Minho, A.S., Arbilla, G., Quiterio, S.L., Escaleira, V., 2014. Trace metals in PM_{10} and $PM_{2.5}$ samples collected in a highly industrialized chemical/petrochemical area and its urbanized surroundings. Bull. Environ. Contam. Toxicol. 92, 590. https://doi.org/10.1007/s00128-014-1219-4.
Prefettura Potenza. 2013. Available in Italian at http://www.prefettura.it/FILES/AllegatiPag/1219/Descrizione%20processo_unit%20Stabilimento%202013.pdf (last access January 2017).
Rager, J.E., Lichtveld, K., Ebersviller, S., Smeester, L., Jaspers, I., Sexton, K.G., Fry, R.C., 2011. A toxicogenomic comparison of primary and photochemically altered air pollutant mixtures. Environ. Health Perspect. 119, 1583–1589.
Reche, C., Querol, X., Alastuey, A., Viana, M., Pey, J., Moreno, T., Rodrìguez, S., Gonzàlez, Y., Fernàndez-Camacho, R., Sànchez de la Campa, A.M., de la Rosa, J., Dall'Osto, M., Prèvôt, A.S.H., Hueglin, C., Harrison, R.M., Quincey, P., 2011. New considerations for PM, black carbon and particle number concentration for air quality monitoring across different European cities. Atmos. Chem. Phys. 11, 6207–6227.
Rutter, A.P., Griffin, R.J., Cevik, B.K., Shakya, K.M., Gong, L., Kim, S., Flynn, J.H., Lefer, B.L., 2015. Sources of air pollution in a region of oil and gas exploration downwind of a large city. Atmos. Environ. 120, 89–99.
Sakari, M., 2012. Depositional history of polycyclic aromatic hydrocarbons: reconstruction of petroleum pollution record in Peninsular Malaysia. In: Puzyn, Tomasz (Ed.), Organic Pollutants Ten Years after the Stockholm Convention—environmental and Analytical Update, ISBN 978-953-307-917-2. InTech.
Sarnela, N., Jokinen, T., Nieminen, T., Lehtipalo, K., Junninen, H., Kangasluoma, J., Hakala, J., Taipale, R., Schobesberger, S., Sipilä, M., Larnimaa, K., Westerholm, H., Heijari, J., Kerminen, V.-M., Petäiä, T., Kulmala, M., 2015. Sulphuric acid and aerosol particle production in the vicinity of an oil refinery. Atmos. Environ. 119, 156–166.
Semeniuk, T.A., Bruintjes, R., Salazar, V., Breed, D., Jensen, T., Buseck, P.R., 2015. Processing of aerosol particles within the Habshan pollution plume. J. Geophys. Res. Atmos. 120, 1996–2012. https://doi.org/10.1002/2014JD022279.
Speranza, A., Caggiano, R., Margiotta, S., Trippetta, S., 2014. A novel approach to comparing simultaneous size-segregated particulate matter (PM) concentration ratios by means of a dedicated triangular diagram using the Agri Valley PM measurements as an example. Nat. Hazards Earth Syst. Sci. 14, 2727–2733. https://doi.org/10.5194/nhess-14-2727-2014.
Stohl, A., Klimont, Z., Eckhardt, S., Kupiainen, K., Shevchenko, V., Kopeikin, V., Novigatsky, A., 2013. Black carbon in the Arctic: the underestimated role of gas flaring and residential combustion emissions. Atmos. Chem. Phys. 13 (17), 8833–8855.
Sudheer, A.K., Rengarajan, R., 2012. Atmospheric mineral dust and trace metals over urban environment in western India during winter. Aerosol Air Qual. Res. 12, 923–933.
Schwarz, J., Cusack, M., Karban, J., Chalupníčková, E., Havránek, V., Smolík, J., Ždíma, V., 2016. $PM_{2.5}$ chemical composition at a rural background site in Central Europe, including correlation and air mass back trajectory analysis. Atmos. Res. 176–177, 108–120.
Trippetta, S., Caggiano, R., Sabia, S., 2014. PM_1 measurements at a site close to an oil/gas pre treatment plant (Agri Valley—southern Italy): a preliminary study. Nat. Hazards Earth Syst. Sci. 14, 2337–2346.
Vecchi, R., Marcazzan, G., Valli, G., Ceriani, M., Antoniazzi, C., 2004. The role of atmospheric dispersion in the seasonal variation of PM1and $PM_{2.5}$ concentration and composition in the urban area of Milan (Italy). Atmos. Environ. 38, 4437–4446.
Warneke, C., Geiger, F., Edwards, P.M., Dube, W., Pétron, G., Kofler, J., Zahn, A., Brown, S.S., Graus, M., Gilman, J.B., Lerner, B.M., Peischl, J., Ryerson, T.B., de Gouw, J.A., Roberts, J.M., 2014. Volatile organic compound emissions from the oil and natural gas industry in the Uintah Basin, Utah: oil and gas well pad emissions compared to ambient air composition. Atmos. Chem. Phys. 14, 10977–10988. https://doi.org/10.5194/acp-14-10977-2014.
Xie, R.K., Seip, H.M., Leinum, J.R., Winje, T., Xiao, J.S., 2005. Chemical characterization of individual particles (PM_{10}) from ambient air in Guiyang City, China. Sci. Total Environ. 343 (1), 261–272.
Zielinska, B., Campbell, D., Samburova, V., 2014. Impact of emissions from natural gas production facilities on ambient air quality in the Barnett Shale area: a pilot study. J. Air & Waste Manag. Assoc. 64 (12), 1369–1383. https://doi.org/10.1080/10962247.2014.954735.